crystals

MDPI

Article

Transition Metals Meet Scorpiand-like Ligands

Salvador Blasco *, Begoña Verdejo, María Paz Clares * and Enrique García-España

Instituto de Ciencia Molecular, Departamento de Química Inorgánica, Universidad de Valencia, C/Catedrático José Beltrán Martínez, 2, 46980 Paterna, Valencia, Spain; begona.verdejo@uv.es (B.V.); enrique.garcia-es@uv.es (E.G.-E.)

* Correspondence: salvador.blasco@uv.es (S.B.); m.paz.clares@uv.es (M.P.C.)

Abstract: Scorpiand-like ligands combine the preorganization of the donor atoms of macrocycles and the degrees of freedom of the linear ligands. We prepared the complexes of several of these ligands with transition metal ions and made a crystallographic and water solution speciation studies. The analysis of the resulting crystal structures show that the ligands have the ability to accommodate several metal ions and that the coordination geometry is mostly determined by the ligand. Ligand 6-[3,7-diazaheptyl]-3,6,9–triaza-1-(2,6)-pyridinacyclodecaphane (**L3**) is an hexadentate ligand that affords a family of isostructural crystals with Cu(II), Mn(II), Ni(II) and Zn(II). The attempts to obtain Co(II) crystals afforded the Co(III) structures instead. Ligand 6-[4-(2-pyridyl)-3-azabutyl]-3,6,9-triaza-1(2,6)-pyridinacyclodecaphane (**L2**) is very similar to **L3** and yields structures similar to it, but its behavior in solution is very different due to the different interaction with protons. Ligand 6-(2-aminoethyl)-3,6,9–triaza-1-(2,6)-pyridinacyclodecaphane (**L1**) is pentadentate and its complexes allow the metal to be more accessible from the solvent. A Zn(II) structure with **L1** shows the species $[ZnBrH\mathbf{L1}]^{2+}$, which exists in a narrow pH range.

Keywords: transition metals; metal ions; coordination chemistry; isostructural; scorpiand-like ligands

Citation: Blasco, S.; Verdejo, B.; Clares, M.P.; García-España, E. Transition Metals Meet Scorpiand-like Ligands. *Crystals* **2023**, *13*, 1338. https://doi.org/10.3390/cryst13091338

Academic Editor: Jesús Sanmartín-Matalobos

Received: 28 July 2023
Revised: 19 August 2023
Accepted: 29 August 2023
Published: 1 September 2023

1. Introduction

Macrocyclic ligands offer an interesting framework for the study of coordination chemistry because all their donor atoms come preorganized, arranged geometrically in space. When they coordinate transition metals, the resulting coordination geometry is determined by the combined action of the preferred coordination geometry of the metal and the ability of the ligand to adapt to it. In the case of macrocyclic ligands, they tend to impose their coordination mode. If the ligand is open, linear and flexible, it has many more conformational degrees of freedom and, therefore, it is able to adapt to a wider variety of coordination preferences. It is possible to combine both types in a family of ligands that features a macrocyclic core decorated with a flexible pending arm containing additional donor atoms. Such ligands are often referred to as scorpiands due to its similarity with the body of a scorpion, where the macrocycle would be the scorpion body and the pending arm would be the tail with a sting at the end of it. They were first reported by Lotz and Kaden [1] although the name scorpiand was first coined by Fabrizzi and collaborators [2].

In our research group, we work with a family of ligands of this kind. Some of them are derivatives of **L1** (see Figure 1), which can be readily obtained from a modified Richman–Atkins condensation of 2,6-bis(bromomethyl)pyridine with tris[2-(*N*-tolylsulphonylaminoethyl)]-amine followed by detosylation with HBr/acetic acid to obtain the hydrobromide salt [3]. **L1** consists of a 12-membered ring with four nitrogen donor atoms: one is a pyridine nitrogen, two of them are secondary amino groups, and the last one is a tertiary amino group. This macrocycle is too small to equatorially coordinate a metal atom. Instead, when a metal atom goes into the cavity, the macrocycle folds leave two adjacent coordination vacancies as it can be seen in the literature in many examples that contain either **L1** or the analog macrocycle without the pending arm [4–7]. This tendency to fold

makes the bonds around N2 and N4 (see numbering in Figure 1) stretched out if it is possible. This feature is relevant in order to understand the structures presented in this work. From the synthetic point of view, **L1** contains a primary amino group, which allows to easily introduce additional moieties in that position. A sizable number of derivatives of **L1** containing different groups in that position have been synthesized and reported by our group [3,8–10]. When **L1** is reacted with 2-pyridinecarboxaldehyde, we obtain the ligand **L2**, which incorporates a sixth donor nitrogen atom in the pending arm. If the reagent is 3-bromopropylphthalimide followed by phthalimide cleavage with hydrazine, we obtain **L3**, which also features a sixth donor atom but is much more flexible than the analog **L2**.

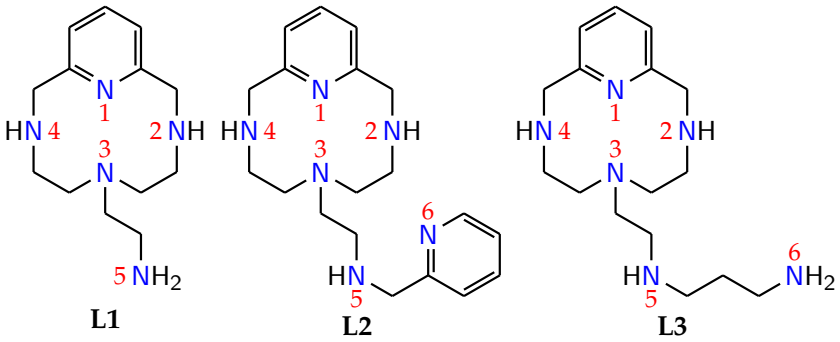

Figure 1. Ligands used in this work and nitrogen atom numbering.

These ligands are able to coordinate many types of metal atoms, mainly transition and post-transition metal ions. So far, we reported interactions with Cu, Mn, Zn, Fe and Pb [3,9,11–13], and research is underway with other metal ions as well. We focused on the copper and manganese complexes of these ligands because they show very interesting redox properties. When the metal in question is able to catalyze one-electron redox reactions, such as Cu(II) or Mn(II), we report that such complexes are able to mimic the redox cycle of superoxide dismutase (SOD), catalyzing the dismutation of the superoxide anion [8,9,11] Iron complexes of **L2** undergo oxidative dehydrogenation by the effect of a pH change [13]. These kinds of metal complexes might seem simple at first glance, but they exhibit a rather complex chemistry. Herein, we aim to present some of the features of this family of complexes by showing both solution and solid-state data in order to illustrate the interesting coordination chemistry that they exhibit.

2. Materials and Methods

2.1. Synthesis and Materials Used

The synthesis of **L1**, **L2** and **L3** was carried out as described in the literature [3,8,9] For crystal preparation and potentiometric measurements, stock solutions ca. 0.1 M of either $MnSO_4 \cdot H_2O$, $Cu(ClO_4)_2 \cdot 6\,H_2O$, $Ni(ClO_4)_2 \cdot 6\,H_2O$, $Zn(ClO_4)_2 \cdot 6\,H_2O$ or $CoCl_2 \cdot 2\,H_2O$ were prepared in Mili-Q water. The metal concentration was standardized by a suitable complexation volumetry method. In the particular case of iron stock solutions, they were prepared from $FeSO_4 \cdot 7\,H_2O$ in 0.1 M HCl. In these cases, both the metal concentration and the acid concentration were determined by volumetric titration. The complexes were prepared by the simple mixing of equimolar amounts of both the metal stock solution and the desired ligand in an aqueous solution. Single crystals were prepared by the slow evaporation of a pH neutral water solution of the corresponding complex. **Caution:** *Perchlorates are potentially explosive if they come in contact with organic matter, and they should be handled with extreme care.*

2.2. X-ray Single Crystal Diffractometry

Single crystal X-ray diffraction was carried out with either of the following machines: (1) Enraf-Nonius KAPPA CCD single-crystal diffractometer with MoK_α radiation ($\lambda = 0.710\,73$ Å) and a graphite monochromator with data collection by COLLECT software with utilities DENZO and SCALEPACK, or (2) Agilent Super-Nova Diffractometer with

MoK_α radiation ($\lambda = 0.710\,73$ Å) with a mirror monochromator located at the Institute of Molecular Sciences (ICMOL) from the University of Valencia, and data acquisition and treatment performed with CRYSALISPRO software [14]. If an absorption correction needed to be applied, either a spherical absorption correction as implemented in DENZO, or a semi-empirical absorption correction (MULABS [15] as implemented in PLATON [16]) was applied.

Crystals were measured at room temperature (293 K). The structures were solved initially with SHELXS [17] with direct methods. Then, they were refined with SHELXL [17] using OLEX2 [18] as the frontend. Final figures for publishing were produced using CHIMERA [19] or MERCURY [20].

2.3. Potentiometric Measurements

The potentiometric titrations were carried out in a thermostated bath at 298.1 K, using $NaClO_4$ 0.15 M as the supporting electrolyte, in the pH range 2.5–11.0. The experimental procedure (burette, potentiometer, cell, stirrer, microcomputer, etc.) is fully described elsewhere [21]. The acquisition of the electromotive force *emf* data was performed with the computer program `PASAT` [22,23]. The reference electrode was an Ag/AgCl electrode in saturated KCl solution. The glass electrode was calibrated as a hydrogen ion concentration probe by titration of previously standardized amounts of HCl with carbonate-free NaOH solutions and the equivalent point determined by the Gran's method [24,25], which gives the standard potential $E^\ominus$ and the ionic product of water ($pK_w = 13.73(1)$). At least two reproducible titrations for each system were recorded. The computer program `HYPERQUAD` [26] was used to fit protonation and stability constants. The independent titration curves were treated first as separate curves, and then the curves for each system (at least two) were then merged and treated as a single set without significant variations in the values of those treated first as separate curves and then merged and treated as a single set without stability constants. The final values were those obtained from the simultaneous treatment of the merged curves. The `HYSS` [27] program was used to generate the distribution diagrams.

3. Results and Discussion

*3.1. Interaction of **L3** with Mn, Fe, Co, Cu, Ni and Zn*

L3 has six donor atoms that can be geometrically arranged in an octahedral disposition. When a metal atom is placed inside the ligand cavity, the ligand itself will impose its preferred coordination geometry rather than the metal. We prepared crystals of **L3** with several transition and post-transition metals and successfully solved the structures for Mn(II), Cu(II), Ni(II) and Zn(II) with ClO_4^- counterions. We named these structures **C1** to **C4**, respectively. Unfortunately, crystals of **L3** with iron could not be obtained. Also, for the case of the Co(II) complex, the Co(III) structure was obtained instead. This ligand readily coordinates metal ions. We studied some metal atoms from the first transition series for their biological relevance. We previously reported copper- or manganese-related crystal structures [9–11], but we include some of them here again for comparative purposes.

We studied metal complex formation in solution and we fitted the values of the formation constants. The results are summarized in Table 1. The stability constant values follow the expected order: Mn < Fe < Cu > Zn. All of them form stable complexes with **L3**. In addition to that, several protonation constants for each complex were also found and refined with up to three protons. The values of the first protonation constants lie between 4.59 for Cu(II) and 8.14 for Fe(II). This indicates that above pH ca. 8, the complex should be completely hexacoordinated. Distribution diagrams show that the species $[ML]^{2+}$ is completely formed in those conditions. Indeed, we obtained all the crystals for **L3** from moderately alkaline solutions. Also, some hydroxylated species were also found in the speciation study, but they only predominate at pH > 11. Solution studies with Ni(II) were also carried out, but the slow kinetics prevented the fitting of reliable formation constants. Nonetheless, suitable single-crystals were obtained from the solutions used in potentiometric measurements. Similarly, solution studies with Co(II) were also carried out,

but the values obtained do not match the expected results probably due to the oxidation that happens during the titration, preventing the collection of reliable data.

Table 1. Formation constants for **L3** with some metal ions from the first transition series.

Reaction [1]	Mn(II) [2]	Fe(II)	Cu(II)	Zn(II)
$MH_2L + H \rightleftharpoons MH_3L$	—	6.35(7) [3]	3.1(2)	4.26(6)
$MHL + H \rightleftharpoons MH_2L$	5.79(9)	5.87(5)	3.59(7)	5.32(3)
$ML + H \rightleftharpoons MHL$	7.74(1)	8.17(2)	4.47(2)	6.27(3)
$M + L \rightleftharpoons ML$	10.93(1)	13.29(4)	22.90(2)	17.72(3)
$ML + H_2O \rightleftharpoons LMOH + H$	−10.74(2)	—	−10.64(4)	−10.53(4)

[1] Charges omitted. [2] Values from ref [9]. [3] Values represent $\log_{10} K$, values in parentheses represent standard deviation of the last significant figure.

Crystals **C1**–**C4** are isostructural (Figure 2a–d) with the same orthorhombic crystal system, P*bca* space group and atom arrangement, with the only difference being the metal atom coordinated to the ligand. Bond distances and angles are shown in Table A4. We always find that the longest bond distances involve N2 and N4. These two donor atoms are the ones that have to stretch more in order to coordinate a metal located inside the macrocycle. When the metal in question displays Jahn–Teller distortion, such as Cu(II) (crystal **C2**, Figure 2b), then the elongated axis is N2—M—N4 so that the bonds around N2 and N4 are in a more relaxed conformation. Some others, like Zn(II), do not have Jahn–Teller distortion but still have the axis N2—M—N4 as being slightly longer. This indicates that the coordination geometry is to a large extent imposed by the ligand and only to a lesser extent by the metal atom. The metal atom, though, also exerts some influence; that is why the length difference between the axial and equatorial bonds is larger for Cu(II) than for Zn(II). In these four structures, the packing is mainly ionic. In Figure 2e, details of the packing of **C1** show the arrangement of anions and cations in the unit cell. It is worthwhile noting that in all these structures, the metal ion is completely wrapped and enclosed by the ligand, leaving no vacant coordination sites and restricted access to the metal from the solvent. This is best seen in Figure 2f, where the spacefill representation shows that the metal ion is not accessible from the solvent. This feature explains that Mn(II) complexes are not oxidized in alkaline conditions open to air, and crystals containing Mn(II) are obtained. When crystals are prepared from a neutral solution of $[MnL1]^{2+}$, then a structure containing Mn(III) is obtained, which consists of two units of $[MnL1]^{3+}$ bridged by an oxo anion [28].

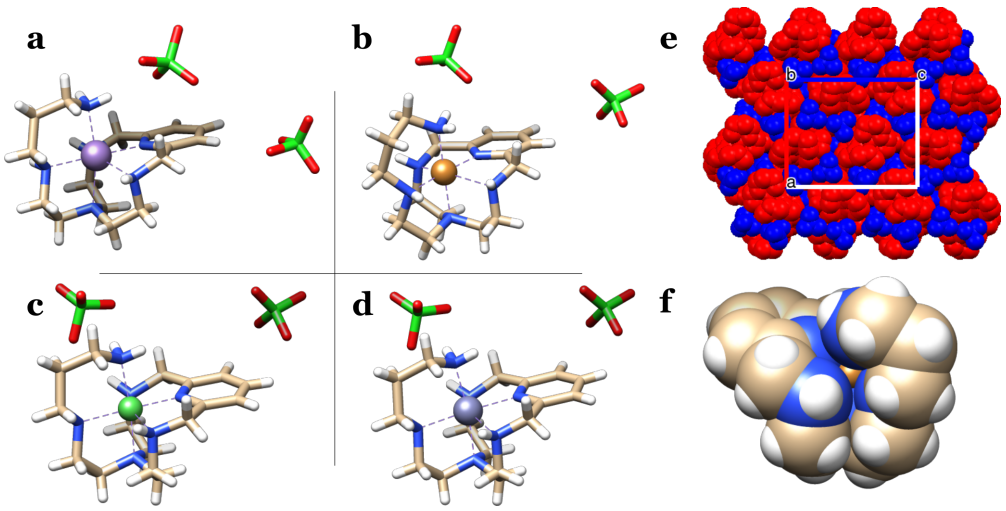

Figure 2. (**a**–**d**) Asymmetric unit of structures **C1**–**C4** featuring Mn(II), Cu(II), Ni(II) or Zn(II), respectively. (**e**) Packing of **C1** with $[CuL3]^{2+}$ depicted in red, and perchlorate anions in blue. (**f**) Spacefill of **C4** highlighting the inaccessibility of the metal atom from the solvent.

*3.2. Cobalt Complexes of **L1** and **L3***

When a pale pink, diluted solution of [Co**L3**]$^{2+}$ in aqueous $NaClO_4$ was allowed to slowly evaporate, deep blue crystals of [Co**L3**]$(ClO_4)_3(H_2O)$ were obtained instead of the expected Co(II) ones. As we noted above, the metal atom inside the cavity was completely enclosed by the ligand, which provides protection against air oxidation for the Mn(II) complexes. This seems not to be the case for Co(II), as we consistently obtained the crystal with Co(III). As mentioned above, speciation studies under argon were carried out, but the obtained formation constants are not reported herein, as the oxidation appears to happen to some extent during the titration process, which makes the values unreliable. A similar thing also happens when Co(II) complexes of **L1** are allowed to slowly evaporate: single crystals containing the [CoBr**L1**]$^{2+}$ complex are obtained. Two different structures containing this complex were resolved: firstly, crystal **C6** with formula [CoBr**L1**]$Br_2(H_2O)$, and crystal **C7** with formula [CoBr**L1**]$Na(ClO_4)_3$ in which sodium perchlorate is co-crystallized along with the complex. In all three examples, the Co(II) atom is easily oxidized to Co(III) by exposure to the atmosphere. The geometry of the complex [CoBr**L1**]$^{2+}$ from **C6** and that of the complex [Co**L3**]$^{3+}$ from **C5** are shown in Figure 3a,b. The complex from [CoBr**L1**]$^{2+}$ from **C7** is not shown, but it is identical to that from **C6**. In all three structures, the Co(III) complex displays an octahedral coordination geometry, fairly regular with angles close to 90° (see Table A5). In the case of **C6** and **C7**, the sixth coordination site is occupied by a bromide atom, which exhibits a longer bond than the others (ca. 2.3 Å), which is to be expected since it is an atom bigger than the other ones. The complex from structure **C7** is essentially identical to that of **C6** with bonds and angles that are only slightly different (see Table A5). As occurs for **C1**–**C4**, the metal atom is deeply embedded, and it has no access from the solvent. In this case, a single water molecule is found in the asymmetric unit along with three perchlorate anions. Structure **C6** contains a rich network of hydrogen bonds involving the hydrogen atoms of the amino groups, the water moiety and the bromide atoms (see Figure 3c). This structure is not purely electrostatic, but also the hydrogen bonds contribute to the packing. The water molecule is placed between two bromide atoms, Br2 and Br3, to which it donates hydrogen bonds, while not accepting from any other moiety. All N—H groups are hydrogen bond donors towards the nearest bromide anion. **C7** is similar to **C6**, but it features an anionic moiety of $(Na(ClO_4)_3)_n^{2n-}$ that grows along the *b* crystallographic axis. Units of [CoBr**L1**]$^{2+}$ cations are placed in alternating orientation, filling in the gaps (see Figure 3d). This structure has a bigger electrostatic contribution to the packing but still some relevant hydrogen bonds are found (see Table A8).

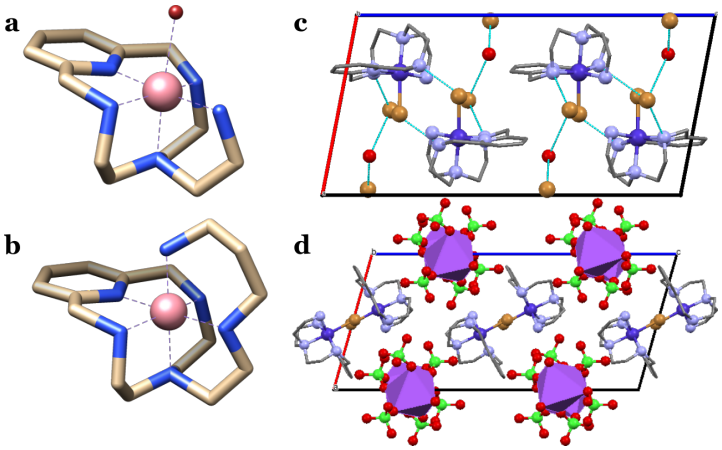

Figure 3. (**a**) Details of the complex [CoBr**L1**]$^{2+}$ from **C6**. Hydrogen atoms not shown. (**b**) Detail of the complex [Co**L3**]$^{3+}$ from **C5**. Hydrogen atoms not shown. (**c**) Unit cell of **C6** shown along the *b*-axis, displaying the packing and the internal hydrogen bonding structure. Hydrogen atoms not shown. (**d**) Unit cell of **C7** shown along the *b*-axis with Na atoms displayed in polyhedral, carbon atoms in capped stick representation, and other atoms displayed in ball-and-stick. Hydrogen atoms not shown.

3.3. Complexes of **L2** with Cu(II) and Mn(II)

From the coordination point of view, **L2** and **L3** are similar because the two of them are hexadentate with the donor atoms in the same positions with the same number of bonds separating one from another. The only difference is that the donor N of **L2** is on a rigid aromatic group and, for **L3**, it is located on a flexible aliphatic amino group. Indeed, the slow evaporation of an aqueous solution of the ligand with one equivalent of either $Cu(ClO_4)_2$ or $Mn(ClO_4)_2$ yields single crystals of either [M**L2**]$(ClO_4)_2$] (**C1** and **C2**) and [M**L3**]$(ClO_4)_2$] (**C8** and **C9**). The coordination mode is almost identical, as it can be seen comparing Figure 2a,b with Figure 4a,b. **C1**, **C2**, **C8** and **C9** crystallize in an orthorhombic system with very similar asymmetric units containing only one molecule of the complex, two perchlorate anions and no water molecules. The space group is different: **C1** and **C2**, which contain **L3**, have a P*bca* space group, while structures **C8** and **C9** have P$na2_1$. Indeed, **C8** is isostructural with **C9** as **C1** is to **C2**. This indicates that the metal exerts little influence outside the complex with regard to the packing. Another similarity is that the packing is mainly electrostatic as it can be seen in Figure 4c. The bond distances and angles are listed in Table A6. We observe, as we did for **L3**, the recurring feature that the longest metal–nitrogen bond distance involves N2 and N4. This is very clear for **C8**, which contains Cu(II). For **C9**, which contains Mn(II), the bond Mn1—N5 is slightly longer than Mn1—N4. A possible explanation for this is that the angles for **C9** are more distorted and further from 90° than for **C8**.

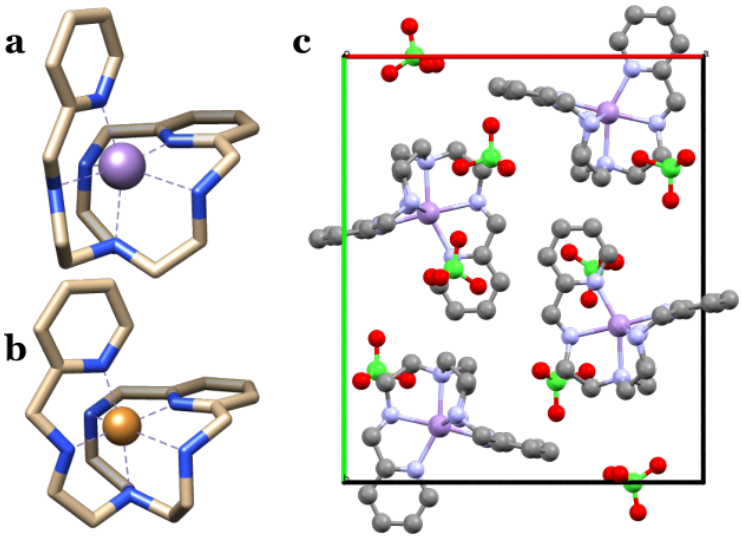

Figure 4. (**a**) Details of the complex $[MnL2]^{2+}$ from **C8**. (**b**) Details of the complex $[CuL2]^{2+}$ from **C9**. (**c**) Unit cell of **C8** viewed down *c* axis. Hydrogen atoms omitted. Mn (purple), Cl (green), O (red), N (blue), C (gray).

If we explore the chemistry in solution, the similarities end, and we see very different behavior compared to the crystal state. Above, in Table 1, we show the formation constants of **L3** with Cu(II). If we study the speciation of **L2** with Cu(II), a single constant is found, with value $\log_{10} K_{CuL} = 22.6(1)$ [29]. This value is very close to that from **L3** ($\log_{10} K_{CuL} = 22.93(2)$, see Table 1). Only this single constant is found, and its large value makes it possible for the species $[CuL]^{2+}$ to be formed at low pH values and predominate in a very large pH range (Figure 5left). This is also the reason for the larger error in the constant: only a small set of points at low pH values contain meaningful information about the formation of the complex (see Figure 5left). Nonetheless, the obtained value is confirmed by means of titration with a competing ligand in order to increase the number of data points [29]. For **L3**, on the other hand, even though the formation constant with Cu(II) is close to that of **L2**, the primary amino group can protonate more easily. As a result,

the Cu(II) atom is introduced at ca. one unit of pH higher, and the species $[Cu\mathbf{L3}]^{2+}$ is not completely formed until pH ∼ 6 (Figure 5right).

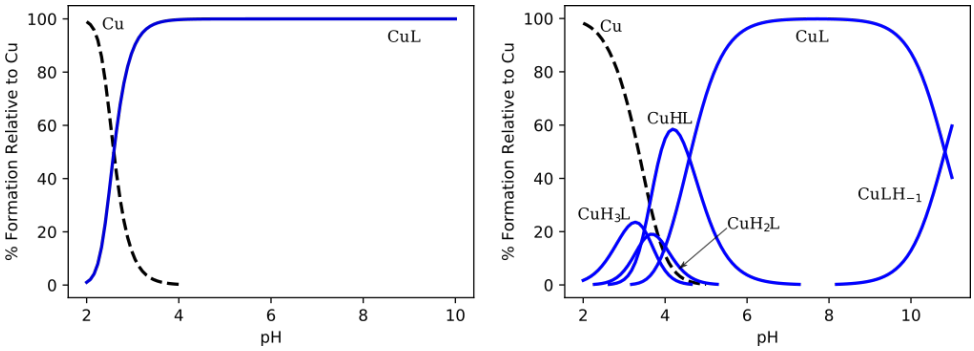

Figure 5. Species distribution diagram for the system Cu(II) with **L2** (**left**) and **L3** (**right**) with $[Cu^{2+}] = [\mathbf{L}] = 1 \times 10^{-3}$ M. Charges omitted.

*3.4. Complex of **L1** with Zn(II)*

L1 is a good ligand for many transition metal atoms, such as Cu(II) [3], Mn(II) [28] or Zn(II) [12]. Usually in all the crystal structures of **L1** reported by us, the metal atom is pentacoordinated with all donor atoms bonding the metal. Solution studies indicate that the complex $[Zn\mathbf{L1}]^{2+}$ can take one or two protons to form species $[ZnH\mathbf{L1}]^{3+}$ and $[ZnH_2\mathbf{L1}]^{4+}$ [12].

We were able to obtain single crystals of one such species, $[ZnH\mathbf{L1}]^{3+}$. This structure, named **C10**, is shown in Figure 6. The terminal amino group can be protonated more easily than the other amino groups, and that coordination bond can break. In this case, the tip of the tail would be +1, while the metal next to it is +2. Therefore, the tail would fold away from the metal, giving, as a result, an open conformation, with the metal much more exposed to the solvent. **C10** presents a triclinic $P\bar{1}$ system and space group, and its asymmetric unit contains the complex $[ZnBrH\mathbf{L1}]^{2+}$ with one water molecule and one $ZnBr_4^{2-}$ counterion. In the unit of $[ZnBrH\mathbf{L1}]^{2+}$, the Zn(II) is pentacoordinated by the nitrogen atoms of **L1**, except N5, which is protonated, bearing one positive charge and being folded away from the metal atom, thus minimizing the electrostatic repulsion. The macrocycle is only partly folded as if it was trying to equatorially coordinate the metal ion but, being too small to do it, it stops halfway. The aforementioned electrostatic repulsion may also contribute to this conformation. N5 would be the fifth donor atom, but instead, a bromide anion fills this vacancy. The units of $[ZnBrH\mathbf{L1}]^{2+}$ are grouped in pairs that share two hydrogen bonds between N4 and Br1 (see Figure 6b). A total of six hydrogen bonds can be located around each unit of complex. The details are shown in Table A9. Both electrostatic and hydrogen bonds are the main forces in the packing. The origin of $ZnBr_4^{2-}$ is the free metal available at pH ∼ 5, where the complex is not completely formed and the bromide counterions are from the **L1** hydrobromide salt.

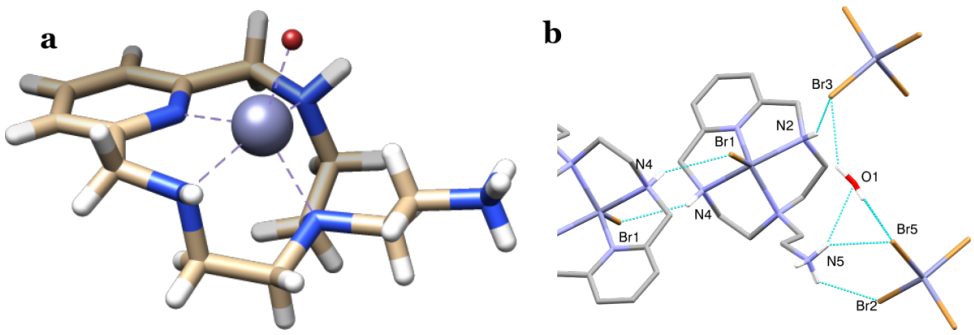

Figure 6. (**a**) Details of the complex $[ZnBrH\mathbf{L1}]^{2+}$ from **C10**. (**b**) Hydrogen bonding network around the complex.

4. Conclusions

The ligands presented herein have the ability to coordinate a variety of metal ions. We focused on metals from the first transition series and showed examples of Cu(II), Mn(II), Co(III), and Ni(II), as well as the post-transition metal ion Zn(II). The overall packing is mostly determined by the ligand. The same ligand with different metal atoms tends to yield either isostructural or structurally similar crystals provided that the charge does not change. **L2** and **L3** have almost the same coordination geometry and, as a consequence, the structures they afford are very similar. However, solid-state structures and solution studies show different pictures about the properties of the complexes due to the different interaction of the ligands with protons as it can be seen by comparing the speciation of Cu(II) and Mn(II) with either **L2** or **L3**. **L1**, which is pentadentate, leaves the metal atom more exposed to the solvent.

Author Contributions: Conceptualization, S.B.; resources, B.V. and M.P.C.; data curation, S.B.; writing—original draft preparation, S.B.; writing—review and editing, S.B. and E.G.-E.; visualization, S.B.; supervision, E.G.-E.; funding acquisition, E.G.-E. All authors have read and agreed to the published version of the manuscript.

Funding: Financial support from the Spanish Ministerio de Economía y Competitividad (Project PID 2019-110751RD-I00) and the Conselleria de Innovación, Universidades, Ciencia y Sociedad Digital of the Generalitat Valenciana (PROMETEO Grant CIPROM/2021/030) is acknowledged.

Data Availability Statement: Crystallographic data have been deposited in the Cambridge Structural Database. These data can be obtained free of charge via http://www.ccdc.cam.ac.uk/conts/retrieving.html accessed on 25 August 2023 (or from the CCDC, 12 Union Road, Cambridge CB2 1EZ, UK; Fax: +44 1223 336033; E-mail: deposit@ccdc.cam.ac.uk). See deposition numbers in Table A1.

Conflicts of Interest: The authors declare no conflict of interest.

Abbreviations

The following abbreviations are used in this manuscript:

SOD	Superoxide dismutase
CCDC	Cambridge Crystallographic Data Center
emf	Electromotive force

Appendix A. Additional Tables

Appendix A.1. Crystallographic Data Tables

Table A1. Deposition numbers of crystal structures **C1–C10** in the Cambridge Crystallographic Data Center.

Structure	CCDC n.	Reference(s)
C1	1020483	[9,11]
C2	897979	[10]
C3	2281410	this work
C4	2281411	this work
C5	2281412	this work
C6	2281413	this work
C7	2281414	this work
C8	888624	[9]
C9	1423684	[29]
C10	2281415	this work

Table A2. Crystallographic data for structures **C3**–**C5**. Values in parentheses represent standard deviation of the last significant figure.

	C3	**C4**	**C5**
Formula	$C_{16}H_{30}Cl_2NiN_6O_8$	$C_{16}H_{30}Cl_2ZnN_6O_8$	$C_{16}H_{32}Cl_3CoN_6O_{13}$
d calc./g cm^{-3}	1.596	1.599	1.756
μ/mm^{-1}	1.108	1.315	1.053
Formula Weight	564.07	570.73	681.75
Colour	pale red	colourless	dark blue
Shape	prism	prism	block
Size/mm^3	0.20 × 0.11 × 0.09	0.14 × 0.11 × 0.09	0.20 × 0.10 × 0.10
Crystal System	orthorrhombic	orthorrhombic	monoclinic
Space Group	P*bca*	P*bca*	P2$_1$/*c*
a/Å	17.4035(5)	17.3510(4)	16.9810(10)
b/Å	12.6487(6)	12.7480(8)	9.2817(4)
c/Å	21.3344(9)	21.4350(9)	21.4350(9)
β/°			109.954(2)
V/Å^3	4696.4(3)	4741.2(4)	2578.5(3)
Z	8	8	4
θ_{max}/°	27.428	27.088	28.101
θ_{min}/°	3.021	3.334	1.276
Measured Refl.	9766	9615	9850
Independent Refl.	5325	5189	5759
R_{int}	0.0529	0.0580	0.0619
Parameters	298	298	356
Restraints	0	0	5
Largest Peak	0.609	0.652	1.036
Deepest Hole	−0.533	−0.528	−0.614
GooF	0.983	1.017	1.021
wR_2 (all data)	0.2460	0.2409	0.2367
wR_2	0.2004	0.1784	0.1975
R_1 (all data)	0.1464	0.1505	0.1418
R_1	0.0699	0.0684	0.0767

Table A3. Crystallographic data for structures **C6**, **C7** and **C10**. Values in parentheses represent standard deviation of the last significant figure.

	C6	**C7**	**C10**
Formula	$C_{13}H_{25}Br_3CoN_5O$	$C_{13}H_{23}BrCoN_5Cl_3NaO_{12}$	$C_{13}H_{24}BrN_5OZn_2$
d calc./g cm^{-3}	2.016	2.028	2.224
μ/mm^{-1}	7.539	2.804	10.398
Formula Weight	566.04	709.54	798.68
Colour	blue	violet	colourless
Shape	spear	block	prism
Size/mm^3	0.70 × 0.44 × 0.32	0.50 × 0.30 × 0.30	0.33 × 0.17 × 0.11
Crystal System	monoclinic	monoclinic	triclinic
Space Group	P2$_1$/*c*	P2$_1$/*c*	P$\bar{1}$
a/Å	10.2042(3)	10.7720(3)	8.1632(2)
b/Å	9.3402(2)	9.6220(6)	10.6612(3)
c/Å	19.9239(6)	23.2950(11)	14.4818(4)
α/°			107.3420(15)
β/°	100.9050(14)	105.792(3)	91.8500(16)
γ/°			96.3360(18)
V/Å^3	1864.64(9)	2323.4(2)	1192.88(6)
Z	4	4	2
θ_{max}/°	25.000	27.490	27.498
θ_{min}/°	2.416	2.285	2.017

Table A3. *Cont.*

	C6	C7	C10
Measured Refl.	18009	9309	26571
Independent Refl.	3282	5271	5472
R_{int}	0.1045	0.0708	0.0733
Parameters	225	333	237
Restraints	3	0	2
Largest Peak	2.032	1.615	1.372
Deepest Hole	−2.621	−1.835	−1.465
GooF	1.028	0.999	1.022
wR_2 (all data)	0.2578	0.2650	0.0983
wR_2	0.2419	0.2321	0.0881
R_1 (all data)	0.0896	0.1415	0.0671
R_1	0.0764	0.0813	0.0396

Appendix A.2. Tables of Distances and Angles

Table A4. Bond distances (Å) and angles (°) for complexes of **L3**.

Bond/Angle	C1 (M=Mn)	C2 (M=Cu)	C3 (M=Ni)	C4 (M=Zn)
M—N1	2.216(4)	2.043(6)	2.024(4)	2.110(5)
M—N2	2.298(5)	2.389(6)	2.203(5)	2.246(5)
M—N3	2.267(5)	2.103(5)	2.113(4)	2.203(5)
M—N4	2.345(5)	2.337(6)	2.179(5)	2.278(6)
M—N5	2.255(4)	2.028(6)	2.105(5)	2.150(6)
M—N6	2.213(5)	2.031(6)	2.099(5)	2.119(5)
N1—M—N2	71.80(18)	76.3(2)	79.23(19)	76.3(2)
N1—M—N3	99.98(18)	91.4(2)	94.95(17)	93.9(2)
N1—M—N4	73.15(18)	77.5(2)	79.3(2)	75.9(2)
N1—M—N5	175.81(18)	176.1(2)	178.2(2)	175.6(2)
N1—M—N6	93.77(19)	91.2(2)	90.1(2)	93.3(2)
N2—M—N3	78.23(18)	79.3(2)	81.80(18)	81.2(2)
N2—M—N4	133.93(19)	147.1(2)	152.77(19)	144.9(2)
N5—M—N2	111.05(19)	103.0(2)	100.94(19)	103.2(2)
N6—M—N2	106.19(19)	97.2(2)	96.2(2)	103.5(2)
N3—M—N4	79.42(18)	81.9(2)	83.53(18)	79.7(2)
N5—M—N3	77.9(2)	84.7(2)	83.28(19)	81.7(2)
N6—M—N3	166.25(19)	175.0(3)	174.1(2)	172.2(2)
N5—M—N4	102.83(17)	101.9(2)	100.0(2)	102.9(2)
N6—M—N4	105.03(19)	102.8(2)	100.43(19)	99.1(2)
N6—M—N5	88.38(19)	92.7(2)	91.7(2)	91.1(2)

Table A5. Bond distances (Å) and angles (°) for complexes of the Co(III) structures. Values in parentheses represent standard deviation of the last significant figure.

C5		C6		C7	
Co1—N1	1.913(4)	Co1—N1	1.889(8)	Co1—N1	1.892(6)
Co1—N2	2.017(4)	Co1—N2	1.983(8)	Co1—N2	2.007(6)
Co1—N3	1.962(4)	Co1—N4	1.967(8)	Co1—N3	1.985(6)
Co1—N4	2.026(4)	Co1—N3	1.985(8)	Co1—N4	2.011(6)
Co1—N5	2.012(4)	Co1—N5	1.951(9)	Co1—N5	1.956(6)
Co1—N6	1.950(5)	Co1—Br4	2.3371(19)	Co1—Br1	2.3600(13)

Table A5. *Cont.*

C5		**C6**		**C7**	
N1—Co1—N4	82.03(17)	N1—Co1—Br4	89.1(2)	N1—Co1—Br1	87.07(17)
N1—Co1—N2	83.91(17)	N1—Co1—N2	83.1(3)	N1—Co1—N2	83.1(3)
N1—Co1—N3	96.97(18)	N1—Co1—N4	97.0(3)	N1—Co1—N3	97.1(2)
N1—Co1—N6	84.41(19)	N1—Co1—N3	83.6(3)	N1—Co1—N4	83.0(3)
N5—Co1—N4	97.75(18)	N2—Co1—Br4	95.1(2)	N2—Co1—Br1	93.98(18)
N5—Co1—N2	96.52(18)	N4—Co1—N2	86.1(3)	N3—Co1—N2	86.4(3)
N3—Co1—N4	86.20(18)	N4—Co1—N3	86.1(3)	N3—Co1—N4	86.5(3)
N3—Co1—N2	85.41(18)	N3—Co1—Br4	94.1(2)	N4—Co1—Br1	94.24(18)
N3—Co1—N5	84.18(19)	N5—Co1—Br4	87.4(2)	N5—Co1—Br1	89.91(18)
N6—Co1—N4	91.4(2)	N5—Co1—N2	96.4(4)	N5—Co1—N2	97.7(3)
N6—Co1—N2	97.32(19)	N5—Co1—N4	86.6(3)	N5—Co1—N3	85.9(3)
N6—Co1—N5	94.4(2)	N5—Co1—N3	97.5(3)	N5—Co1—N4	96.7(3)

Table A6. Bond distances (Å) and angles (°) for complexes of **L2**. Values in parentheses represent standard deviation of the last significant figure.

C8 (M=Cu)		**C9 (M=Mn)**	
Cu1—N1	2.031(11)	Mn1—N1	2.165(6)
Cu1—N2	2.26(3)	Mn1—N2	2.333(16)
Cu1—N3	2.114(12)	Mn1—N3	2.256(11)
Cu1—N4	2.368(18)	Mn1—N4	2.26(2)
Cu1—N5	1.962(11)	Mn1—N5	2.266(13)
Cu1—N6	2.011(11)	Mn1—N6	2.173(10)
N1—Cu1—N2	78.7(11)	N1—Mn1—N2	73.6(6)
N1—Cu1—N3	93.2(4)	N1—Mn1—N3	102.7(3)
N1—Cu1—N4	78.6(10)	N1—Mn1—N4	72.2(7)
N2—Cu1—N4	150.8(6)	N1—Mn1—N5	166.2(6)
N3—Cu1—N2	84.5(10)	N1—Mn1—N6	103.9(3)
N3—Cu1—N4	78.6(9)	N3—Mn1—N2	81.2(6)
N5—Cu1—N1	178.7(8)	N3—Mn1—N4	76.9(7)
N5—Cu1—N2	100.5(13)	N3—Mn1—N5	79.2(5)
N5—Cu1—N3	85.7(5)	N4—Mn1—N2	133.6(4)
N5—Cu1—N4	101.8(12)	N4—Mn1—N5	95.2(7)
N5—Cu1—N6	82.4(5)	N5—Mn1—N2	120.1(7)
N6—Cu1—N1	98.8(4)	N6—Mn1—N2	111.0(7)
N6—Cu1—N2	97.2(12)	N6—Mn1—N3	153.0(4)
N6—Cu1—N3	168.0(4)	N6—Mn1—N4	106.9(7)
N6—Cu1—N4	104.3(10)	N6—Mn1—N5	73.9(5)

Appendix A.3. Tables of Hydrogen Bonds

Table A7. Hydrogen bond data for **C6**. Symmetry operations: (i) $1-x$, $-y$, $1-z$; (ii) x, $\frac{1}{2}-y$, $\frac{1}{2}+z$. Distances in Å, angles in °. Values in parentheses represent standard deviation of the last significant figure.

		Distances		**Angle**
D—H···A [1]	**D—H**	**H···A**	**D···A**	**D—H···A**
N5—H5A···Br2^{i}	0.89	2.88	3.659(8)	146
O1—H1A···Br2^{i}	0.83(13)	2.86(13)	3.355(11)	120(10)
O1—H1B···Br3^{i}	0.81(6)	2.58(7)	3.368(11)	164(7)
N2—H2···Br2^{i}	0.98	2.32	3.295(8)	174
N5—H5B···Br2^{ii}	0.89	2.57	3.427(8)	160
N4—H4···Br2^{ii}	0.98	2.44	3.384(8)	161
N5—H5C···Br2^{i}	0.89	2.82	3.659(8)	157
N5—H5D···Br2^{i}	0.89	2.64	3.427(8)	147

[1] D = donor, H = hydrogen, A = acceptor.

Table A8. Hydrogen bond data for **C7**. Symmetry operations: (i) $1-x, 1-y, 1-z$. Distances in Å, angles in °. Values in parentheses represent standard deviation of the last significant figure.

		Distances		Angle
D—H···A [1]	**D—H**	**H···A**	**D···A**	**D—H···A**
N2—H2A···O13^{i}	0.98	2.23	3.125(10)	152
N4—H4A···Br1^{i}	0.98	2.39	3.346(7)	165
N5—H5A···O13^{i}	0.89	2.11	2.945(10)	155
N5—H5B···Br1^{i}	0.89	2.70	3.476(7)	147

[1] D = donor, H = hydrogen, A = acceptor.

Table A9. Hydrogen bond data for **C10**. Symmetry operations: (i) $1-x, y, z$; (ii) $1-x, 1-y, -z$; (iii) $1-x, 2-y, 1-z$; (iv) $1-x, 1+y, z$. Distances in Å, angles in °. Values in parentheses represent standard deviation of the last significant figure.

		Distances		Angle
D—H···A [1]	**D—H**	**H···A**	**D···A**	**D—H···A**
O1—H1C···Br3^{i}	0.81(4)	2.62(8)	3.290(14)	141(9)
O1—H1D···Br5^{ii}	0.83(11)	2.50(10)	3.324(13)	175(9)
N2—H2 ···Br3^{i}	0.98	2.53	3.440(4)	155
N4—H4 ···Br1^{iii}	0.98	2.71	3.550(4)	144
N5—H5A···Br2^{ii}	0.89	2.67	3.364(6)	135
N5—H5B···Br4^{iv}	0.89	2.48	3.316(6)	158
N5—H5C···O1	0.89	2.50	3.277(16)	147
N5—H5C···Br5^{ii}	0.89	2.93	3.637(6)	138

[1] D = donor, H = hydrogen, A = acceptor.

References

1. Lotz, T.J.; Kaden, T.A. pH-Induced co-ordination geometry change in a macrocyclic nickel (II) complex. *J. Chem. Soc. Chem. Commun.* **1977**, *1*, 15–16. [CrossRef]
2. Pallavicini, P.S.; Perotti, A.; Poggi, A.; Seghi, B.; Fabbrizzi, L. N-(aminoethyl) cyclam: A tetraaza macrocycle with a coordinating tail (scorpiand). Acidity controlled coordination of the side chain to nickel (II) and nickel (III) cations. *J. Am. Chem. Soc.* **1987**, *109*, 5139–5144. [CrossRef]
3. Verdejo, B.; Ferrer, A.; Blasco, S.; Castillo, C.E.; González, J.; Latorre, J.; Máñez, M.A.; Basallote, M.G.; Soriano, C.; García-España, E. Hydrogen and copper ion-induced molecular reorganizations in scorpionand-like ligands. A potentiometric, mechanistic, and solid-state study. *Inorg. Chem.* **2007**, *46*, 5707–5719. [CrossRef] [PubMed]
4. Johnston, H.M.; Palacios, P.M.; Pierce, B.S.; Green, K.N. Spectroscopic and solid-state evaluations of tetra-aza macrocyclic cobalt complexes with parallels to the classic cobalt(II) chloride equilibrium. *J. Coord. Chem.* **2016**, *69*, 1979–1989. [CrossRef]
5. Félix, V.; Costa, J.; Delgado, R.; Drew, M.G.B.; Duarte, M.T.; Resende, C. X-Ray diffraction and molecular mechanics studies of 12-, 13-, and 14-membered tetraaza macrocycles containing pyridine: Effect of the macrocyclic cavity size on the selectivity of the metal ion. *J. Chem. Soc. Dalton Trans.* **2001**, 1462–1471. [CrossRef]
6. Magallón, C.; Griego, L.; Hu, C.H.; Company, A.; Ribas, X.; Mirica, L.M. Organometallic Ni(ii), Ni(iii), and Ni(iv) complexes relevant to carbon–carbon and carbon–oxygen bond formation reactions. *Inorg. Chem. Front.* **2022**, *9*, 1016–1022. [CrossRef]
7. Cavalleri, M.; Panza, N.; di Biase, A.; Tseberlidis, G.; Rizzato, S.; Abbiati, G.; Caselli, A. [Zinc(II)(Pyridine-Containing Ligand)] Complexes as Single-Component Efficient Catalyst for Chemical Fixation of CO_2 with Epoxides. *Eur. J. Org. Chem.* **2021**, *2021*, 2764–2771. [CrossRef]
8. Castillo, C.E.; Máñez, M.A.; Basallote, M.G.; Clares, M.P.; Blasco, S.; García-España, E. Copper (II) complexes of quinoline polyazamacrocyclic scorpiand-type ligands: X-ray, equilibrium and kinetic studies. *Dalton Trans.* **2012**, *41*, 5617–5624. [CrossRef]
9. Clares, M.P.; Serena, C.; Blasco, S.; Nebot, A.; del Castillo, L.; Soriano, C.; Domenech, A.; Sánchez-Sánchez, A.V.; Soler-Calero, L.; Mullor, J.L.; et al. Mn (II) complexes of scorpiand-like ligands. A model for the MnSOD active centre with high in vitro and in vivo activity. *J. Inorg. Biochem.* **2015**, *143*, 1–8. [CrossRef]
10. Inclán, M.; Albelda, M.T.; Frías, J.C.; Blasco, S.; Verdejo, B.; Serena, C.; Salat-Canela, C.; Díaz, M.L.; García-España, A.; García-España, E. Modulation of DNA Binding by Reversible Metal-Controlled Molecular Reorganizations of Scorpiand-like Ligands. *J. Am. Chem. Soc.* **2012**, *134*, 9644–9656. [CrossRef]
11. Clares, M.P.; Blasco, S.; Inclán, M.; del Castillo Agudo, L.; Verdejo, B.; Soriano, C.; Doménech, A.; Latorre, J.; García-España, E. Manganese (II) complexes of scorpiand-like azamacrocycles as MnSOD mimics. *Chem. Commun.* **2011**, *47*, 5988–5990. [CrossRef] [PubMed]

12. González, J.; Llinares, J.M.; Belda, R.; Pitarch, J.; Soriano, C.; Tejero, R.; Verdejo, B.; García-España, E. Tritopic phenanthroline and pyridine tail-tied aza-scorpiands. *Org. Biomol. Chem.* **2010**, *8*, 2367–2376. [CrossRef] [PubMed]
13. Clares, M.P.; Acosta-Rueda, L.; Castillo, C.E.; Blasco, S.; Jimenez, H.R.; Garcia-Espana, E.; Basallote, M.G. Iron (II) Complexes with Scorpiand-Like Macrocyclic Polyamines: Kinetico-Mechanistic Aspects of Complex Formation and Oxidative Dehydrogenation of Coordinated Amines. *Inorg. Chem.* **2017**, *56*, 4400–4412. [CrossRef]
14. *CrysAlisPro*, Version 1.171.36.28; Agilent Technologies: Santa Clara, CA, USA, 2012.
15. Blessing, R.H. An empirical correction for absorption anisotropy. *Acta Crystallogr. A* **1995**, *51*, 33–38. [CrossRef] [PubMed]
16. Spek, A.L. Structure validation in chemical crystallography. *Acta Crystallogr. D* **2009**, *65*, 148–155. [CrossRef] [PubMed]
17. Sheldrick, G.M. Crystal structure refinement with SHELXL. *Acta Crystallogr. C* **2015**, *C71*, 3–8. [CrossRef]
18. Dolomanov, O.; Bourhis, L.; Gildea, R.; Howard, J.; Puschmann, H. Olex2—A complete package for Molecular Crystallography. *J. Appl. Crystallogr.* **2009**, *42*, 339–342. [CrossRef]
19. Pettersen, E.F.; Goddard, T.D.; Huang, C.C.; Couch, G.S.; Greenblatt, D.M.; Meng, E.C.; Ferrin, T.E. UCSF Chimera—A visualization system for exploratory research and analysis. *J. Comput. Chem.* **2004**, *25*, 1605–1612. [CrossRef]
20. Macrae, C.F.; Sovago, I.; Cottrell, S.J.; Galek, P.T.; McCabe, P.; Pidcock, E.; Platings, M.; Shields, G.P.; Stevens, J.S.; Towler, M.; et al. Mercury 4.0: From visualization to analysis, design and prediction. *J. Appl. Crystallogr.* **2020**, *53*, 226–235. [CrossRef]
21. Garcia-España, E.; Ballester, M.J.; Lloret, F.; Moratal, J.M.; Faus, J.; Bianchi, A. Low-spin six-coordinate cobalt(II) complexes. A solution study of tris(violurato)cobaltate(II) ions. *J. Chem. Soc. Dalton Trans.* **1988**, 101–104. [CrossRef]
22. Fontanelli, M. In *Proceedings of the I Spanish-Italian Congress on Thermodynamics of Metal Complexes, Castellón, Spain, 1990*; Diputación de Castellón: Castellón, Spain, 1990.
23. Savastano, M.; Fiaschi, M.; Ferraro, G.; Gratteri, P.; Mariani, P.; Bianchi, A.; Bazzicalupi, C. Sensing Zn^{2+} in Aqueous Solution with a Fluorescent Scorpiand Macrocyclic Ligand Decorated with an Anthracene Bearing Tail. *Molecules* **2020**, *25*, 1355. [CrossRef] [PubMed]
24. Gran, G. Determination of the equivalence point in potentiometric titrations. Part II. *Analyst* **1952**, *77*, 661–671. [CrossRef]
25. Rossotti, F.; Rossotti, H. Potentiometric titrations using Gran plots: A textbook omission. *J. Chem. Ed.* **1965**, *42*, 375. [CrossRef]
26. Gans, P.; Sabatini, A.; Vacca, A. Investigation of equilibria in solution. Determination of equilibrium constants with the HYPERQUAD suite of programs. *Talanta* **1996**, *43*, 1739–1753. [CrossRef]
27. Alderighi, L.; Gans, P.; Ienco, A.; Peters, D.; Sabatini, A.; Vacca, A. Hyperquad simulation and speciation (HySS): A utility program for the investigation of equilibria involving soluble and partially soluble species. *Coord. Chem. Rev.* **1999**, *184*, 311–318. [CrossRef]
28. Blasco, S.; Cano, J.; Clares, M.P.; García-Granda, S.; Doménech, A.; Jiménez, H.R.; Verdejo, B.; Lloret, F.; García-España, E. A Binuclear MnIII Complex of a Scorpiand-Like Ligand Displaying a Single Unsupported MnIII–O–MnIII Bridge. *Inorg. Chem.* **2012**, *51*, 11698–11706. [CrossRef]
29. Blasco, S.; Verdejo, B.; Clares, M.P.; Castillo, C.E.; Algarra, A.G.; Latorre, J.; Máñez, M.A.; Basallote, M.G.; Soriano, C.; García-España, E. Hydrogen and Copper Ion Induced Molecular Reorganizations in Two New Scorpiand-Like Ligands Appended with Pyridine Rings. *Inorg. Chem.* **2010**, *49*, 7016–7027. [CrossRef]